Instrument Science Report WFC3 2008-04

WFC3 TV2 Testing: IR Channel Read Noise

B. Hilbert
12 Feb 2008

ABSTRACT

*Using data taken during WFC3's Thermal Vacuum 2 (TV2) testing campaign, we have characterized the readnoise behavior in the IR Channel, which contained IR-1 (FPA129). Data were taken at FPA temperatures of -123°C and -125.4°C, while the nominal on-orbit operating temperature of the IR channel is -128°C. At the lower of the two FPA temperatures, correlated double sampling (CDS) readnoise values varied by quadrant between 15.6 and 19.5 ¯e. Each quadrant appeared to have different temperature sensitivity, with the readnoise value in quadrant 4 changing by over 1 ¯*e for the 2.4*-°C temperature change, versus a change of only 0.1 ¯e for quadrant 1. By combining all 16 reads of a given ramp into a final image, we found values of effective noise between 9.1 – 13.0 ¯e at -125.4°C.*

Introduction

The Wide Field Camera 3 (WFC3) underwent a second round of thermal vacuum testing (TV2) during the summer and autumn of 2007. This testing was completed using the flight spare, IR-1 (FPA129) in the IR channel while the flight detector was under construction. Nevertheless, we used TV2 to characterize the readnoise behavior of IR-1, following much the same testing procedure to be used on the flight detector in TV3.

Data

All of the data collected and analyzed for this study were the products of the Science Mission Specification (SMS) script IR01S13. The SMS was run several times during TV2. Table 1 lists the characteristics of the data collected. All data files had an identical format. Each file contained a data ramp. This ramp was composed of 16 individual reads that sampled the detector at 16 different times during the integration. The timing of these samples is described by the sample sequence name. Petro and Wheeler (2006) describe the sampling scheme for each sequence. For the sequences listed in Table 1, RAPID samples the detector as quickly as possible (2.9 seconds between reads), while the number attached to each SPARS sequence lists the amount of time (in sec) between consecutive reads.

FPA Temp (°C)	**Sample Sequences**	**Number of Ramps**
-123		
	RAPID	6
	SPARS10	5
	SPARS25	3
	SPARS50	3
	SPARS100	5
	SPARS200	6
-125.4		
	RAPID	3
	SPARS10	3
	SPARS25	3
	SPARS50	3
	SPARS100	3
	SPARS200	3

Table 1: Data collected as part of the IR readnoise test during TV2.

Analysis

Prior to analyses, all data ramps were run through several steps of the WFC3 IDL data reduction pipeline (Hilbert, 2004). We used the vertical inboard reference pixels to subtract the bias signal from each ramp. The standard practice of subtracting the initial

read from all subsequent reads in a ramp was not performed. The reason for this is discussed below. Finally, we multiplied each ramp by the gain values derived in TV2, in order to get the data into units of electrons (Hilbert, 2007). No non-linearity corrections were necessary due to the low overall signal levels in the data.

The most commonly quoted readnoise value for multiple readout detectors is the correlated double sampling (CDS) noise. This is the readnoise measured on an image created from the difference of two consecutive reads of the detector. By differencing consecutive reads, we remove pixel-to-pixel variations in the zero level, assuring that they do not contaminate the measure of the readnoise. This technique works best on ramps with short exposure times between reads. The short duration between reads minimizes the amount of dark current that accumulates on the detector. This in turn limits the amount of shot noise in the reads, leaving the readnoise as the dominant noise source.

Upon constructing the consecutive difference frames, each 16-read ramp produced a set of 15 difference images. Our first task was to measure the CDS readnoise in each of these 15 images. We created histograms, on a quadrant-by-quadrant basis, of each difference image, and then used the IDL function MPFITPEAK.pro to fit a Gaussian, and find the width of the distributions. This value was saved as the measured CDS readnoise for that difference image. Figure 1 shows a typical histogram for one quadrant of a difference image. The widths of the histograms were very sensitive to the bin size used in the creation of the histograms. For example, using a bin size of 2.12 versus 2.20 e^- changed the widths of the resulting histograms by up to 0.7 e^-. We chose to use the smallest bin size that produced a smooth distribution for all the histograms; 2.15 e^-. As can be seen in Figure 2 and Table 2, histogram widths, and therefore readnoise values, were consistent to roughly several tenths of an electron along a single ramp. The same is true for median CDS values between ramps of similar sample sequence and temperature.

Figure 2 shows, for a single RAPID ramp, the measured CDS readnoise for all of the 15 difference images. This is a RAPID ramp and is relatively unaffected by shot noise from dark current. Therefore the scatter in the CDS values is dominated by binning and Gaussian fitting effects on the histograms.

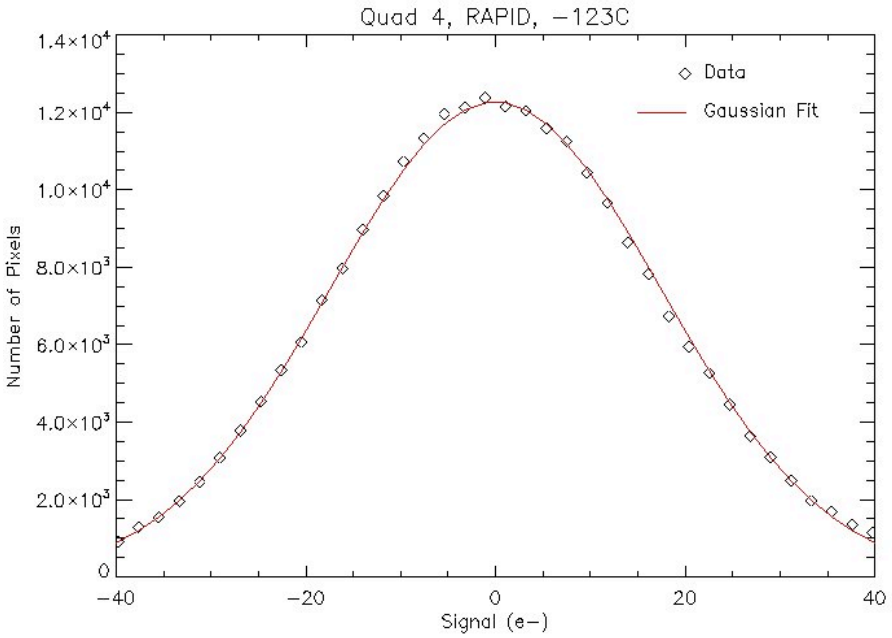

Figure 1: Typical readnoise histogram from the difference of two consecutive reads. The readnoise is the width of the best -fit Gaussian.

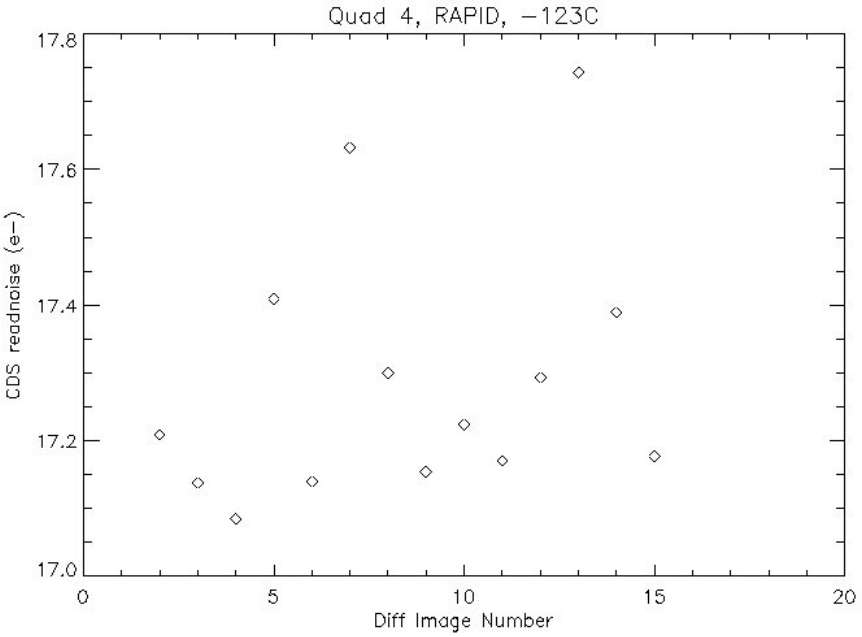

Figure 2: CDS readnoise measured in each difference image associated with a RAPID ramp taken at -123°C.

Table 2 gives the CDS readnoise results for the ramps taken with the RAPID sample sequence as part of the IR01S13 SMS. The readnoise value quoted for each ramp represents the median of the CDS readnoise values calculated for all difference images of

that ramp. Quadrant 1 consistently had the lowest readnoise, followed by quadrant 4. Quadrants 2 and 3 were higher still, and comparable to one another. These are also the two quadrants found to have the lowest dark current rates (Hilbert, 2007). We follow the standard convention of quadrant 1 in the upper left of the detector, and quadrant number increasing in a counter-clockwise direction.

Another interesting result shown here is the degree to which the readnoise is affected by changes in the FPA temperature (recorded in the IRFPATMP header keyword). The measured CDS readnoise in quadrant 1 seems to be nearly independent of FPA temperature, given the typical 0.1 e^- variation observed across ramps. Temperature appeared to have a much larger effect on quadrant 4, where the measured readnoise decreased by ~1 e^- for a 2.4ºC change in temperature. The effects on quadrants 2 and 3 fall between these two extremes.

FPA Temp (ºC)	Quad 1 (e^-)	Quad 2 (e^-)	Quad 3 (e^-)	Quad 4 (e^-)
-123				
	15.64	19.58	19.44	17.19
	15.66	19.42	19.57	17.35
	15.62	19.43	19.49	17.27
	15.58	19.56	19.53	17.30
	15.58	19.60	19.46	17.42
	15.63	19.66	19.44	17.21
-123 Mean	15.62	19.54	19.49	17.29
-125.4				
	15.51	18.92	19.08	16.22
	15.56	18.84	19.18	16.28
	15.58	18.97	19.17	16.21
-125.4 Mean	15.55	18.91	19.15	16.23
Difference between -123ºC and -125.4ºC	0.07	0.63	0.34	1.04

Table 2: Median CDS readnoise values for each of the RAPID ramps. The consistency of readnoise values within a quadrant suggest an uncertainty of several hundredths of an electron. However, given the histogram behavior described in the text, uncertainties are closer to 0.2 – 0.3 e^-.

A second measure of the readnoise was also made for each ramp. For a ramp taken with the WFC3 IR channel, one of the final data products is a "final image", in which the measured signals in the individual reads are used to construct a single image of the measured signal rate. For a ramp with a given sample sequence, and therefore exposure

time, we wished to calculate the effective noise present in the "final image" associated with that ramp. In this case, we are interested in all sample sequences, not only the short RAPID sequence.

In order to calculate this effective noise, we employ a method described by Robberto (priv. communication). In general, line-fitting of the measured signal up the ramp is used to create the "final image". For each pixel, the best-fit slope is recorded as the signal rate. As such, we wished to calculate the noise associated with this best fit slope. In order to accomplish this, we needed to calculate the noise associated with the measured signal in each read, and propagate those noise values through to the "final image".

This was done via a two-step fitting process, on a pixel-by-pixel basis. First, we calculated a best-fit line (using IDL's LINFIT.PRO procedure) to the signal up the ramp, just as if we were creating a "final image". The slope from this best fit was recorded as the dark current rate for that pixel. Knowing the dark current rate, along with the exposure time for each read within the ramp, we were able to calculate the signal in each read due to dark current accumulation. The shot noise associated with this dark current signal was then simply the square root of that signal. The other noise component present in the measured signal was the readnoise. For this, we used the median CDS readnoise values listed in Table 1. These CDS noise values could be translated into single-read readnoise values by dividing by the square root of 2, since CDS images are the difference of 2 reads.

Once we knew the values for the two noise components, we had to combine them in order to obtain a total noise value for each read. However, the readnoise and dark current noise cannot simply be added in quadrature, due to correlation in the dark current values as you travel up the ramp. This implies that the noise associated with the accumulating dark current increases following Equation 1, which was derived by Robberto (2007). Here, *DC* is the measured dark current rate, *t* is the exposure time, and *N* is the number of reads in the ramp (16 in our case).

$$\sigma_{DC} = \sqrt{DC \cdot t \cdot \frac{6}{5}\frac{\left(N^2+1\right)}{\left(N^2-1\right)}} \qquad 1)$$

Combining this equation for the dark current shot noise with the readnoise, we arrive at Equation 2, which describes the total noise, or uncertainty, on the measurement of each signal up the ramp. Here, σ_{CDS} is the CDS readnoise measured using the difference images.

$$\sigma_S = \sqrt{\left(\frac{\sigma_{CDS}}{\sqrt{2}}\right) + \left(DC \cdot t \cdot \frac{6}{5}\frac{\left(N^2+1\right)}{\left(N^2-1\right)}\right)} \qquad 2)$$

With the noise values from Equation 2 in hand, we repeated the line fitting up the ramp. This time, the noise values were entered as the uncertainties associated with the signal values to be fit. In this case, along with the best-fit slope, we were able to calculate the true error on the best-fit slope. All line-fitting was performed on the measured signal versus time, so we took this error on the fitted slope, multiplied by the exposure time of the final read, and produced the effective noise. This entire process was performed on a pixel-by-pixel basis, resulting in a map of the effective noise across the entire detector. Also, as there is no rule stating that the "final image" must be constructed from 16 reads of the detector, we repeated this process, varying the number of reads each time. In other words, we performed the line-fitting first using only the first 4 reads of each ramp, in order to find the effective noise on a 4-read ramp. Next, we used 5 reads, then 6, and so on, in order to monitor how the effective noise decreases with the number of reads. As with the CDS images discussed above, once we had an effective noise map, we produced a histogram, and used a Gaussian fit to find the peak value of the distribution.

We performed this analysis on all RAPID and SPARS ramps from IR01S13, being sure to separate the data taken at an FPA temperature of -123ºC from those taken at -125.4ºC. Table 3 gives the results of the effective noise measurements in quadrant 4 for each type of sample sequence and temperature. The reported noise values represent the median of the effective noise values, calculated on the 3 to 6 ramps in that group. Results for all quadrants can be found in the Appendix.

FPA Temp (ºC)	**Sample Sequence**	**Exposure Time for 3/8/16 reads (sec)**	**Effective Noise 3 Reads (⁻e)**	**Effective Noise 8 reads (⁻e)**	**Effective Noise 16 reads (⁻e)**
-123	RAPID	6 / 21 / 44	16.4	12.5	9.4
	SPARS10	13 / 63 / 143	16.8	12.8	9.8
	SPARS25	28 / 153 / 353	16.3	12.8	9.9
	SPARS50	53 / 303 / 703	16.7	13.4	10.6
	SPARS100	102 / 602 / 1402	17.1	14.1	11.2
	SPARS200	202 / 1202 / 2802	17.1	14.3	11.7
-125.4	RAPID	6 / 21 / 44	16.4	12.5	9.4
	SPARS10	13 / 63 / 143	16.0	12.2	9.3
	SPARS25	28 / 153 / 353	15.2	12.1	9.2
	SPARS50	53 / 303 / 703	15.5	12.4	9.6
	SPARS100	102 / 602 / 1402	15.8	13.0	10.3
	SPARS200	202 / 1202 / 2802	16.7	13.8	11.1

Table 3: Effective noise values for various sample sequences, in quadrant 4 of FPA129.

Figure 3 shows the behavior of the effective noise for one of the SPARS200 ramps. The blue line marks the measured CDS readnoise for the ramp. This value was calculated by taking the difference of the first and second reads (ignoring the reset read), creating a histogram and finding the width of the best-fit Gaussian. As most of these data were not taken using the RAPID sample sequence, the exposure time between these two reads varied with sample sequence, which allowed shot noise from accumulated dark current to contribute to the measured noise. In order to remove the dark current contribution to the noise, we used line-fitting, as described previously, to create a dark current map of the detector. A Gaussian fit to the histogram of this dark current map was used to find the peak dark current value. As the noise values were calculated using the first two reads of the ramp, the dark current noise correction was minimal (on the order of 0.02 e^- in the case of the SPARS200 ramps).

The red curve in Figure 3 displays the effective noise measured in a "final image" created from varying numbers of individual reads. The effect of using multiple reads for noise reduction is powerful. For any sample sequence, the effective noise decreases by 30-40% in using 16 reads versus 3. Reduction of the FPA temperature by 2.4ºC was found to decrease the effective noise values by an additional 0.5 to 1.0 e^-.

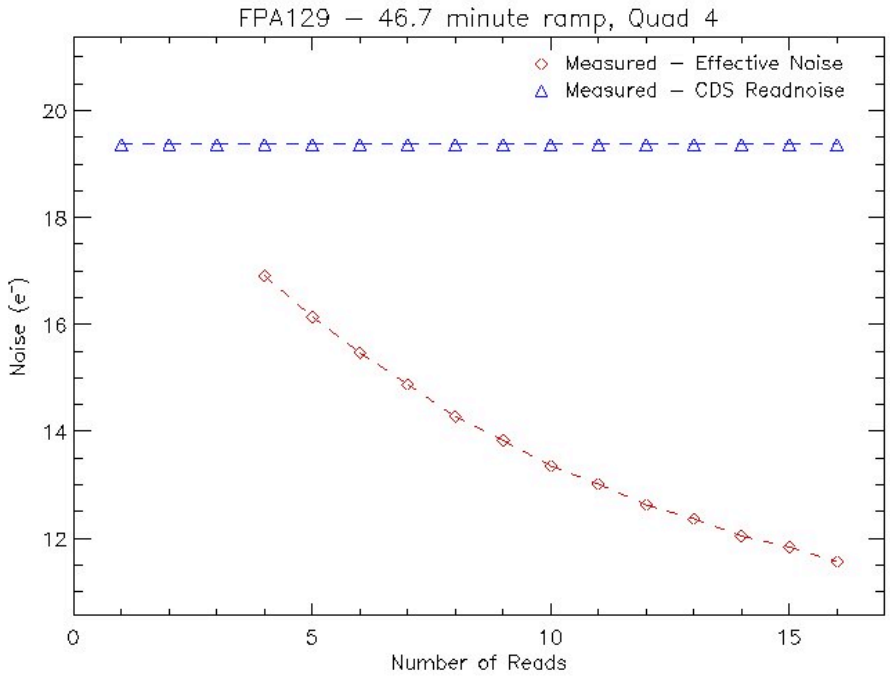

Figure 3: Effective noise for a SPARS200 ramp, taken at an FPA temperature of -123ºC. The "CDS" readnoise measured here is contaminated by dark current shot noise, placing it above the values reported in Table 2.

Conclusions

The readnoise behavior for IR-1 (FPA129) appears fairly complex. CDS readnoise values vary from quadrant to quadrant by roughly 20%, with quadrant 1 having the lowest CDS readnoise, followed by quadrant 4, and then 2 and 3. However, the CDS readnoise also varies with temperature differently for each quadrant. Quadrant 4 seems the most sensitive to changes in FPA temperature, while quadrant 1 is only minimally affected.

Following the standard data reduction practice of creating a final image from the component reads of each ramp, we see that the effective noise for FPA129 decreases significantly for large numbers of reads. This implies that for readnoise-limited observations, maximizing the number of reads in each ramp can be an effective technique for optimizing the signal-to-noise ratio of the data.

Recommendations

Given the complex temperature sensitivity observed in IR-1, new readnoise data for IR-4 should be obtained for any change in operating temperature. Also there were hints that the ramp-to-ramp scatter in effective noise values was greater at -125.4ºC than at -123ºC. However, with only 3 ramps for many of the sample sequences, it was difficult to make statistical arguments. For the flight detector, more data using each sample sequence will help reduce uncertainties.

References

Hilbert, B. ***Basic IDL Data Reduction Algorithm for WFC3 IR and UVIS Channel.*** WFC3 ISR 2004-10. http://www.stsci.edu/hst/wfc3/documents/ISRs/WFC3-2004-10.pdf 10 June 2004.

Hilbert, B. ***WFC3 TV2 Testing: IR Channel Gain Results.*** http://www.stsci.edu/hst/wfc3/documents/ISRs/WFC3-2007-28.pdf 5 Dec 2007.

Hilbert, B. and M. Robberto. ***WFC3-IR Thermal Vacuum Testing: IR Channel Dark Current.*** http://www.stsci.edu/hst/wfc3/documents/ISRs/WFC3-2005-25.pdf 22 Aug 2005.

Petro, L. and T. Wheeler. ***New IR Detector Sample Times.*** http://www.stsci.edu/hst/wfc3/documents/ISRs/WFC3-2006-06.pdf 2 Oct 2006.

Robberto, M. ***Analysis of the sampling schemes for WFC3-IR.*** http://www.stsci.edu/hst/wfc3/documents/ISRs/WFC3-2007-12.pdf 30 Apr 2007.

Appendix

Measured effective noise values for each quadrant of FPA129.

Quadrant 1

FPA Temp (ºC)	Sample Sequence	Exposure Time for 3/8/16 reads (sec)	Effective Noise 3 Reads (e⁻)	Effective Noise 8 reads (e⁻)	Effective Noise 16 reads (e⁻)
-123	RAPID	6 / 21 / 44	15.7	12.0	9.0
	SPARS10	13 / 63 / 143	15.3	11.6	8.9
	SPARS25	28 / 153 / 353	15.1	11.9	9.1
	SPARS50	53 / 303 / 703	15.0	12.1	9.6
	SPARS100	102 / 602 / 1402	15.8	13.0	10.4
	SPARS200	202 / 1202 / 2802	17.1	14.3	11.7
-125.4	RAPID	6 / 21 / 44	15.8	12.0	9.1
	SPARS10	13 / 63 / 143	15.3	11.6	8.9
	SPARS25	28 / 153 / 353	15.1	12.0	9.3
	SPARS50	53 / 303 / 703	14.0	11.2	8.7
	SPARS100	102 / 602 / 1402	15.4	12.6	10.2
	SPARS200	202 / 1202 / 2802	16.3	13.7	11.1

Table 4: Effective noise values for various sample sequences, in quadrant 1 of FPA129.

Quadrant 2

FPA Temp (ºC)	Sample Sequence	Exposure Time for 3/8/16 reads (sec)	Effective Noise 3 Reads (e⁻)	Effective Noise 8 reads (e⁻)	Effective Noise 16 reads (e⁻)
-123	RAPID	6 / 21 / 44	19.7	15.0	11.3
	SPARS10	13 / 63 / 143	19.1	14.6	11.2
	SPARS25	28 / 153 / 353	18.6	14.7	11.3
	SPARS50	53 / 303 / 703	18.5	14.9	11.7
	SPARS100	102 / 602 / 1402	18.3	15.1	12.0
	SPARS200	202 / 1202 / 2802	20.6	17.2	13.9
-125.4	RAPID	6 / 21 / 44	18.8	14.4	10.8
	SPARS10	13 / 63 / 143	18.4	14.0	10.7

	SPARS25	28 / 153 / 353	17.8	14.1	11.0
	SPARS50	53 / 303 / 703	17.8	14.4	11.3
	SPARS100	102 / 602 / 1402	18.3	15.1	11.9
	SPARS200	202 / 1202 / 2802	19.0	15.9	12.9

Table 5: Effective noise values for various sample sequences, in quadrant 2 of FPA129.

Quadrant 3

FPA Temp (ºC)	**Sample Sequence**	**Exposure Time for 3/8/16 reads (sec)**	**Effective Noise 3 Reads (e⁻)**	**Effective Noise 8 reads (e⁻)**	**Effective Noise 16 reads (e⁻)**
-123	RAPID	6 / 21 / 44	19.6	15.0	11.3
	SPARS10	13 / 63 / 143	18.9	14.4	11.0
	SPARS25	28 / 153 / 353	18.3	14.4	11.1
	SPARS50	53 / 303 / 703	18.1	14.6	11.5
	SPARS100	102 / 602 / 1402	17.9	14.7	11.7
	SPARS200	202 / 1202 / 2802	20.3	16.8	13.6
-125.4	RAPID	6 / 21 / 44	19.3	14.8	11.1
	SPARS10	13 / 63 / 143	18.7	14.3	10.9
	SPARS25	28 / 153 / 353	18.2	14.3	11.0
	SPARS50	53 / 303 / 703	17.9	14.4	11.1
	SPARS100	102 / 602 / 1402	18.3	15.0	12.0
	SPARS200	202 / 1202 / 2802	19.2	15.9	12.9

Table 6: Effective noise values for various sample sequences, in quadrant 3 of FPA129.

Quadrant 4

FPA Temp (ºC)	**Sample Sequence**	**Exposure Time for 3/8/16 reads (sec)**	**Effective Noise 3 Reads (e⁻)**	**Effective Noise 8 reads (e⁻)**	**Effective Noise 16 reads (e⁻)**
-123	RAPID	6 / 21 / 44	16.4	12.5	9.4
	SPARS10	13 / 63 / 143	16.8	12.8	9.8
	SPARS25	28 / 153 / 353	16.3	12.8	9.9
	SPARS50	53 / 303 / 703	16.7	13.4	10.6
	SPARS100	102 / 602 / 1402	17.1	14.1	11.2

	SPARS200	202 / 1202 / 2802	17.1	14.3	11.7
-125.4	RAPID	6 / 21 / 44	16.4	12.5	9.4
	SPARS10	13 / 63 / 143	16.0	12.2	9.3
	SPARS25	28 / 153 / 353	15.2	12.1	9.2
	SPARS50	53 / 303 / 703	15.5	12.4	9.6
	SPARS100	102 / 602 / 1402	15.8	13.0	10.3
	SPARS200	202 / 1202 / 2802	16.7	13.8	11.1

Table 7: Effective noise values for various sample sequences, in quadrant 4 of FPA129.